

# A Low-Profile, Wide-Angle, and Bandwidth Enhanced Rectenna for Radiative Energy Harvesting in the 12 GHz Band

Trung Dung Ha, *Graduate Student Member, IEEE*, Xuecong Nie, Hakan Bađcı, *Senior Member, IEEE*, Danilo Erricolo, *Fellow, IEEE*, and Pai-Yen Chen, *Senior Member, IEEE*

**Abstract**— This letter proposes a low-profile rectenna with high gain and wide angular coverage for radio frequency (RF) energy harvesting and wireless power transmission applications. Specifically, a compact traveling-wave antenna (TWA) array with spatially multiplexed radiation patterns is integrated with a miniature rectifying circuit and a DC power combiner, enabling wide angular coverage and stable DC output power. Our numerical and experimental results show that the proposed rectenna can be robust against changes in the received power and the incident angle (from  $-65^\circ$  to  $65^\circ$ , while allowing a wideband operation from 11.5 GHz to 12.5 GHz. The proposed rectenna exhibits a nearly constant DC output voltage of 1.8 V and a RF-to-DC power conversion efficiency of 45% at a power density of  $2.86 \text{ mW/cm}^2$  over a wide range of incident angles and operating frequencies.

**Index Terms**— Radiative energy harvesting, travelling wave antennas, rectifying circuits, rectenna.

## I. INTRODUCTION

THE number of connected smart devices in machine-to-machine (M2M) networks is forecast to be surpassed 80 billion by 2025 [1]. Due to such high demand for massive-device systems, the rectifying antenna (or rectenna) technology has emerged as an effective and sustainable way to harvest energy from ambient electromagnetic waves (i.e., wireless power grids) to power ubiquitous devices and wireless sensor networks connected via 5G/B5G ecosystems. Other potential RF energy harvesting applications include, but are not limited to, self-powering unmanned aerial vehicles, autonomous vehicles [2-4], energy harvesting sensing and communication nodes [5-6], wake-up radios [7-9], low-power wearable and textile electronics [10-13]. So far, many efforts have been made to increase the power conversion efficiency (PCE) and reduce the cost of rectennas used for the long-range (far-field) wireless energy harvesting and power transmission [14-21]. The simplest possible rectenna configuration could be to exploit a compact omnidirectional antenna loaded with nonlinear electronic devices (e.g., diodes) [22-32], to directly rectify the ambient electromagnetic wave into the usable DC electricity.

T. D. Ha, X. C. Nie, D. Erricolo, and P.-Y. Chen are with the Department of Electrical and Computer Engineering, University of Illinois, Chicago, IL 60607 U.S.A.

H. Bađcı is with the Division of Computer Electrical and Mathematical Science and Engineering, King Abdullah University of Science and Technology (KAUST), Thuwal, Saudi Arabia.

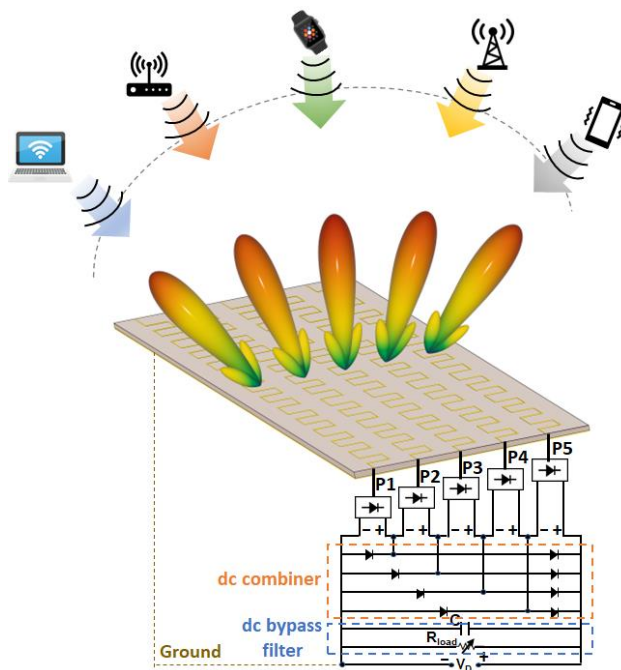


Fig. 1: Schematic diagram of the wideband, wide-angle wireless power transmission and energy harvesting system.

However, the relatively low gain of these antennas results in limited RF power delivered to the rectifier circuit, thereby reducing the PCE. This problem may worsen as the distance from the source increases (i.e. farfield RF energy harvesting), resulting in a lower available incident power density. Recent studies reported the need for a high-gain receiving antenna to compensate for the lower available power density [33-34]. Although directional antennas can mitigate the low received RF power, one drawback is their narrow beamwidth and thus narrow angular coverage. This may pose challenges in practical applications because the relative positioning between the RF source and the energy harvester is usually unknown, resulting in an incident angle-sensitive power conversion efficiency. To date, few studies have explored the trade-off between the

Trung Dung Ha and Xuecong Nie contributed equally to this work. This material is based upon work supported by the National Science Foundation under Grant No. EECS-EPMD 2210977. Corresponding Author: P. Y. Chen; email: [pychen@uic.edu](mailto:pychen@uic.edu)

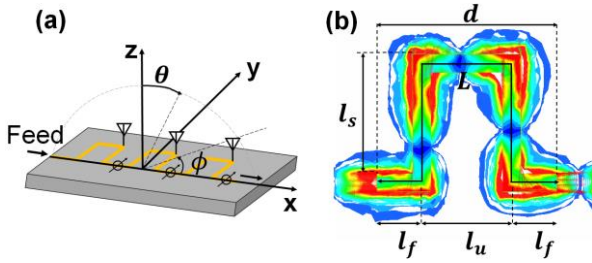


Fig. 2: (a) Perspective view of the proposed travelling-wave antenna. (b) simulated current density distribution of a unit cell at 12 GHz.

antenna gain and the angular coverage in rectenna development [35-40]. A. Eid, *et al.* [38] presented a wide-angle rectenna based on the Rotman lens for 5G mm-wave energy harvesting. This rectenna provided a realized gain of 17 dBi at each port at 28 GHz, with an angular coverage of  $110^\circ (\pm 55^\circ)$ . However, the Rotman lens is rather bulky and has a relatively high loss [41]. Y.-J. Ren, *et al.*, [40] proposed a retrodirective rectenna array that operates at the 5.8 GHz frequency band provided a moderated low gain of 5.89 dBi with a beamwidth of  $\sim 80^\circ$ .

In this letter, we propose a new integrated rectenna design based on a traveling-wave antenna (TWA) array for efficient, wide-angle and wideband RF energy harvesting. Moreover, this rectenna can have a high PCE that is nearly unchanged over a wide range of incident angles in the 12 GHz frequency band. Noticeably, the proposed wide-angle TWA array-based rectenna with  $130^\circ$  coverage can be effective over a frequency range from 11.5 GHz to 12.5 GHz. A self-biased rectifier and a DC power combiner [Fig. 1] are used to deal with the unbalanced rectified DC output power, which occurs in realistic RF energy harvesting scenarios. As a result, the integrated RF energy harvesting device has a stable DC voltage and a reasonably invariant PCE.

## II. TRAVELLING-WAVE ANTENNA ARRAY DESIGN

### A. Design of beam-steering travelling-wave antennas

Fig. 2 shows the geometry and design parameters of the TWA, where short microstrip-line sections of width  $w$  and length  $l_f$  are connected by a U-shaped stub of length  $d = 2l_f + l_u$  and width  $w$ . Each U-shaped stub has sharp corners, which cause leakage radiation and can be considered as a radiating element; the full-wave simulation results for the current distribution of a unit cell are shown in Fig. 2 (b). Besides, in this periodic phase-shifting structure, each unit cell with a total microstrip-line length  $L = 2(l_f + l_u) + l_u$  yields a progressive phase difference, given by  $\Delta\varphi = \beta[2(2l_f + l_u) + l_u]$  where  $\beta$  is the phase constant of the microstrip transmission line [44]. The array factor can be written as

$$AF = e^{-\alpha[(N-1)/2]} e^{j[(N-1)/2]\psi} \frac{\sin\left(\frac{N(\psi + j\alpha)}{2}\right)}{\sin\left(\frac{\psi + j\alpha}{2}\right)} \quad (1)$$

where  $\psi = k_0 d \sin \theta + \Delta\varphi$ ,  $N$  is the number of radiators,  $d$  is the spacing between them,  $\theta$  is the radiation angle,  $k_0$  is the free-space wavenumber,  $\alpha = -\ln|S_{21}| \times L$  is the attenuation

TABLE I  
CALCULATED DIMENSIONS OF TWA AT DIFFERENT RADIATION ANGLE (unit: mm)

Rad. Angle	$l_f$	$l_s$	$l_u$	$L$	$d$
$-60^\circ$	2.75	7.3	5.5	25.6	11
$-30^\circ$	3.05	7.3	6.1	26.8	12.2
$0^\circ$	2.25	3.7	4.5	16.4	9
$30^\circ$	2.95	3.9	5.9	19.6	11.8
$60^\circ$	2.85	4.9	5.7	21.2	11.4

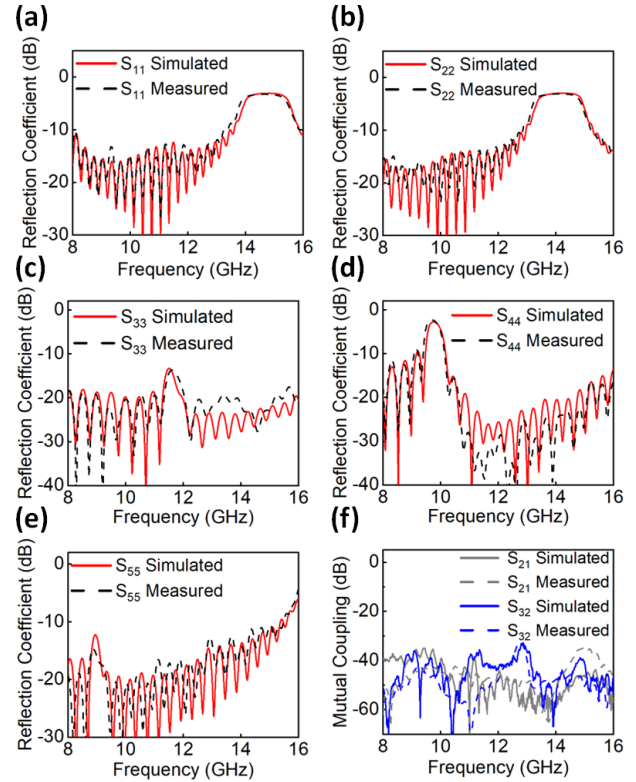


Fig. 3: Simulated (solid) and measured (dashed) reflection coefficient of the directional TWAs in, whose steering angle are: (a)  $-60^\circ$ , (b)  $-30^\circ$ , (c)  $0^\circ$ , (d)  $30^\circ$ , and (e)  $60^\circ$ , and (f) isolation between neighboring antennas in the same rectenna panel.

constant of the transmission line. If value of  $\alpha$  is small, the radiation angle at which the maximum occurs is given by:

$$\theta_0 = \arccos\left(\frac{\Delta\varphi}{k_0 d}\right) \quad (2)$$

The array factor and associated radiation characteristics of a TWA can be varied by adjusting the spacing between adjacent radiating elements. The lengths  $l_f$ ,  $l_u$ , and  $l_s$  must be adjusted accordingly to achieve different radiating angles, as shown in Fig. 1. Here, we consider the Roger RO 4003C substrate with dielectric constant  $\epsilon_r = 3.55$ , loss tangent  $\tan\delta = 0.0027$ , and thickness  $t = 0.5$  mm. The width of the microstrip line is chosen to be  $w = 1.1$  mm such that its characteristic impedance  $Z_0 = 50 \Omega$ . Table 1 summarizes the calculated design parameters of the TWA for different radiation angles ( $-60^\circ$ ,  $-30^\circ$ ,  $0^\circ$ ,  $30^\circ$ , and  $60^\circ$ ) at 12 GHz.

### B. Radiation properties of travelling-wave antennas

According to the design parameters in Table I, a low-profile rectenna panel consisting of five TWAs was built. Each TWA

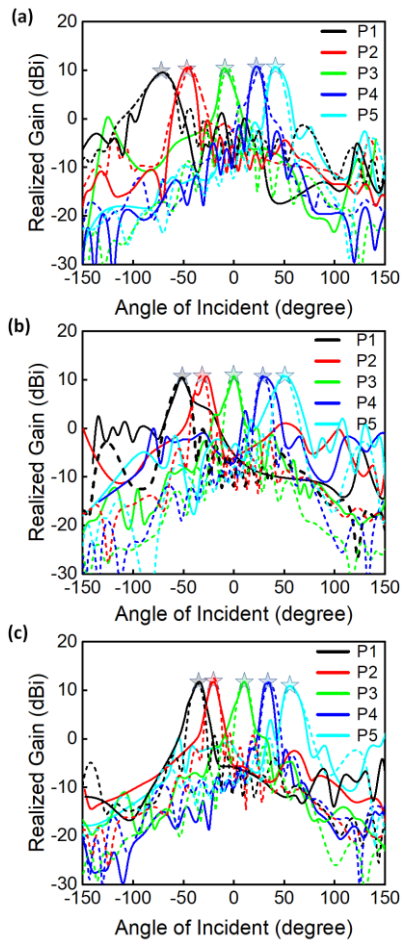


Fig. 4: Measured (solid lines) and simulated (dashed lines) radiation patterns for the TWAs in Fig. 8, operating at (a) 11.5 GHz, (b) 12 GHz, and (c) 12.5 GHz. Here, stars represent calculated results from Eq. (2).

has eleven unit-cells whose dimensions were properly designed to control the steering angle of the main lobe. The number of radiative elements is carefully chosen to guarantee that ~90% of input power leaks into free space [42]. To avoid backward traveling waves, each TWA is terminated with a  $50 \Omega$  dummy load. Figs. 3 (a)-(e) report the simulated and measured reflection coefficients for the five TWAs. The numerical and experimental results show good agreement, but with slight difference due to fabrication errors. It can be seen from Fig. 3 that all TWAs have a moderately broad bandwidth in the frequency range between 11.5 GHz and 12.5 GHz, albeit with different radiation patterns. Fig. 3(f) reports the mutual coupling between TWAs, showing that the mutual coupling related to  $S_{ij}$  can be below  $-37$  dB at frequencies of interest (for brevity, only  $S_{21}$  and  $S_{32}$  are presented).

Figs. 4 (a)-(c) report the simulated and measured H-plane radiation properties of individual TWAs printed on the board at 11.5 GHz, 12 GHz, and 12.5 GHz, respectively; the numerical (dashed lines) and experimental (solid lines) results are in good agreement. Fig. 5 shows the simulated 3-D radiation patterns for the five TWAs operating at 12 GHz, which are excited individually (a)-(e) and simultaneously (f). We find that continuous beam steering can be obtained by adjusting the phase loading of TWAs. Furthermore, design parameters obtained from Eq. (2) can give the targeted radiation angle, as

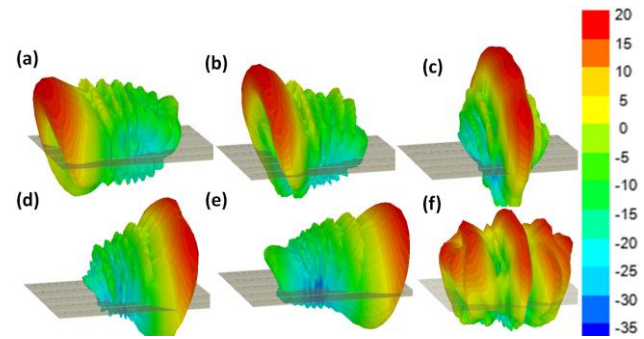


Fig. 5: Simulated 3-D radiation pattern for the rectenna panel, of which TWA are excited individually (a-e) and simultaneously (f) at 12 GHz; units: dBi.

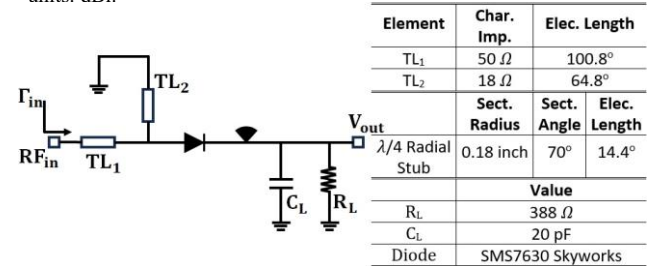


Fig. 6: Schematics and parameters of the half-wave rectifier.

validated by the numerical and experimental results presented in Fig. 4. The analytically estimated radiation angles highlighted as stars in Fig. 4 agree well with the numerical results. According to Eq. (2)-(3), the radiation angle can also be altered by varying the operating frequency. When the operating frequency increases (decreases), the beam is tilted by a positive (negative) angle, as shown in Fig. 4(a) and 4(c). This rectenna panel may cover an angular range spanning from  $-65^\circ$  to  $65^\circ$  continuously at 11.5 GHz to 12.5 GHz. From all operating scenarios in Fig. 4, the average sidelobe level (SLL) remains low ( $< -15$  dB).

### III. DESIGN AND MEASUREMENT OF INTEGRATED RECTENNA

#### A. Design and performance evaluation of rectifiers.

The half-wave rectifying circuit includes a matching network, Schottky diodes, a dc-pass filter, and a resistive load, as sketched in Fig. 6. The zero-bias Schottky diode, Skyworks SMS7630, is chosen for its low forward junction capacitance ( $0.14$  pF), low series resistance ( $20 \Omega$ ), low turn-on voltage, and high reverse saturation current ( $4 \mu\text{A}$ ) [43]. The transmission lines TL<sub>1</sub> and TL<sub>2</sub> are used for the single-stub matching, and their optimum dimensions are defined by the source-pull simulation using the diode's SPICE model SMS7630 from Skyworks. A quarter-wave radial stub is used as an RF choke, which is considered as a short-circuit for second harmonic byproducts of the rectification. R<sub>L</sub> and C<sub>L</sub> act as the DC load and bypass filter connected in shunt with the load. The optimum design parameters of TL<sub>1</sub> and TL<sub>2</sub>, and the radial stub are presented in the inset table of Fig. 6. The rectifier was printed on the same board as the antenna, as shown in the inset of Fig. 7(a). The RF-to-DC power conversion efficiency (PCE) of the rectifier is defined as [16]

$$\eta = \frac{V_o^2}{R_L P_r} \times 100\% \quad (3)$$

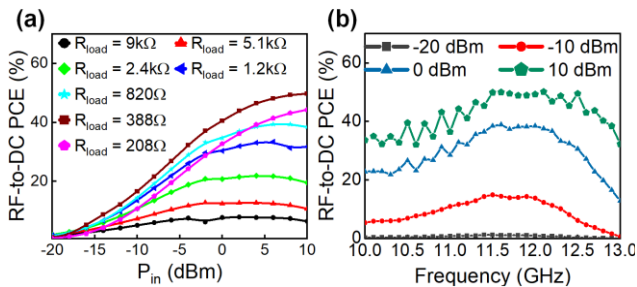


Fig. 7: (a) PCE versus resistive load, and (b) PCE versus frequency (with optimum resistive load) for a rectifier operating at 12 GHz.

where  $V_o$  is the measured output voltage across the resistive load  $R_L$ , and  $P_r$  is the power delivered at the rectifier. Here, the insertion loss between connectors is negligible, and therefore,  $P_r$  is equal to the power delivered to the receiver. Fig. 7 (a) shows the measured RF-to-DC PCE against the input power at 12 GHz under different load resistances ( $R_L$ ). The highest PCE is  $\sim 50\%$  at an input power of 10 dBm, obtained with a load resistance of 388  $\Omega$ . Even at an RF input power of -10 dBm, the measured PCE is still  $\sim 20\%$ . Fig. 7(b) presents the measured PCE against the operating frequency at different input RF power levels. At an RF input power of 10 dBm, the rectifier maintains a PCE of 50% from 11.5 GHz to 12.6 GHz.

### B. Characterization of the integrated RF energy harvester.

The wide-angle rectenna, consisting of an array of TWAs, rectifying circuits, a DC power combiner, a DC pass filter, and a resistive load, was fabricated and characterized. The top and bottom views of the integrated rectenna panel are shown in Figs. 8 (a) and (b), respectively. The received RF signals are rectified into DC current, and eight low-frequency bypass diodes are used for the DC power combiner. The DC power combiner based on low-frequency diodes (Infineon BAT63-02V) can deal with the unbalanced rectification outputs produced by TWAs. The low-pass filter isolate DC components from RF signals.

The integrated rectenna system was measured in free space. The transmitter contains a signal generator with an output power of 30 dBm and a horn antenna. The horn antenna has a peak gain of 19.2 dBi, 19.4 dBi, and 19.6 dBi at 11.5 GHz, 12 GHz, and 12.5 GHz, respectively. The rectenna is 0.5 m away from the transmitter. During the measurement, the rectenna panel was rotated and the dependence of the PCE and output DC voltage on the incident angle  $\theta$  was measured.

By applying the Friis' equation to estimate the received power on the rectenna  $P_r$  [45], Eq. (3) can be rewritten as

$$\eta = \frac{V_o^2 / R_L}{P_r} = \frac{V_o^2 / R_L}{P_t G_t G_r (\lambda_o / 4\pi r)^2} \quad (4)$$

where  $P_t$  represents the transmitted power,  $G_t$  and  $G_r$  are the realized gains of the horn antenna and the TWAs, respectively,  $r$  is the distance between the TX and the rectenna, and  $\lambda_o$  is the wavelength. Figs. 9(a)-(b) report the measured DC output voltage and PCE against the incident angle, respectively; here, the resistive load at the output of the DC combiner is also adjusted to achieve the maximum conversion efficiency. The power density on the rectenna is calculated at 2.86 mW/cm<sup>2</sup>. The output voltage exhibits only a small fluctuation (1.5 V to

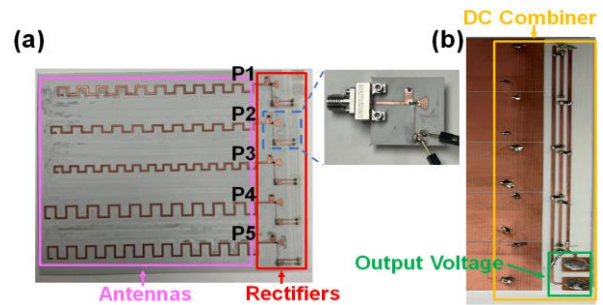


Fig. 8: (a) Top and (b) bottom views of the fabricated rectenna; inset of (a) shows an individual rectifying circuit.

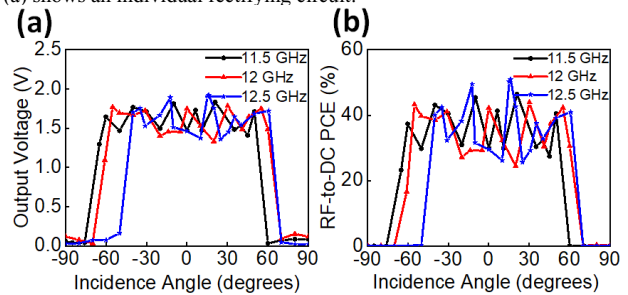


Fig. 9: (a) Dependence of the measured output voltage on the angle of arrival at 11.5 GHz (black lines), 12 GHz (red lines), and 12.5 GHz (blue lines). (b) is similar to (a), but for the PCE calculated using Eq. (4).

1.9 V) over a wide angular range (130°). Moreover, such an effect can be similarly obtained from 11.5 GHz to 12.5 GHz, as can be seen in Fig. 9 (a). When the incident angle exceeds the coverage range, the output voltage drops sharply to millivolt level. Broadening the angular coverage may be achieved by integrating more TWAs to effectively capture endfire and backfire radiation. The RF input power delivered to the rectenna is nearly 12 dBm and the resistive load is fixed at 317  $\Omega$ . Fig. 9(b) reports the RF-to-DC PCE of the integrated rectenna, showing that a maximum PCE of 35% to 50% over a wide angular range of 130° and a frequency range from 11.5 GHz to 12.5 GHz. Similar to Fig. 9(a), the PCE drops when the incident angle exceeds the angular range of coverage. Compared with previously reported wide-angle rectennas [35-40], our design exhibits not only wider angular coverage, but also enhanced bandwidth and compactness. The proposed rectenna may also be fully integrated and low-cost, thus being suitable for practically energy harvesting in the 12 GHz band.

### IV. CONCLUSION

In summary, we have proposed a compact, low-profile, low-cost, and wide-angle rectenna based on the simple microstrip-line traveling-wave structure. The microstrip-line TWAs not only can achieve a 12 dBi gain (which is insensitive to the radiation angle), but also a readily tunable radiation angle. We have designed, fabricated, and characterized the fully integrated rectenna board comprising the TWAs, rectifier, and DC power management circuit with a compact size of 13×10×0.5 cm<sup>3</sup>. Our results show that in the potential 5G mid-band spectrum centered at 12 GHz, the rectenna can provide an 130° angular coverage, an average output voltage of 1.8 V, and an average RF-to-DC PCE of 45% (insensitive to the incident angle) at a power density of 2.86 mW/cm<sup>2</sup>.

REFERENCES

- [1] A. Zanella, N. Bui, A. Castellani, L. Vangelista, and M. Zorzi, "Internet of Things for smart cities," *IEEE Internet Things J.*, vol. 1, no. 1, pp. 22–32, Feb. 2014.
- [2] K. Niotaki, A. Collado, A. Georgiadis, S. Kim, and M. M. Tentzeris, "Solar/electromagnetic energy harvesting and wireless power transmission," *Proc. IEEE*, vol. 102, no. 11, pp. 1712–1722, Nov. 2014.
- [3] K. Huang and V. K. N. Lau, "Enabling wireless power transfer in cellular networks: Architecture, modeling and deployment," *IEEE Trans. Wireless Commun.*, vol. 13, no. 2, pp. 902–912, Feb. 2014.
- [4] H. Yan, Y. Chen, and S.-H. Yang, "UAV-Enabled wireless power transfer with base station charging and UAV power consumption," *IEEE Trans. Veh. Technol.*, vol. 69, no. 11, pp. 12883–12896, Nov. 2020.
- [5] S. Kim, A. Georgiadis, A. Collado, and M. M. Tentzeris, "An inkjet-printed solar-powered wireless beacon on paper for identification and wireless power transmission applications," *IEEE Trans. Microw. Theory Techn.*, vol. 60, no. 12, pp. 4178–4186, Dec. 2012.
- [6] N. B. Carvalho et al., "Wireless power transmission: R&D activities within Europe," *IEEE Trans. Microw. Theory Techn.*, vol. 62, no. 4, pp. 1031–1045, Apr. 2014.
- [7] R. Piyare, A. L. Murphy, C. Kiraly, P. Tosato, and D. Brunelli, "Ultralow power wake-up radios: A hardware and networking survey," *IEEE Commun. Surveys Tuts.*, vol. 19, no. 4, pp. 2117–2157, 4th Quart., 2017.
- [8] H. Bello, Z. Xiaoping, R. Nordin, and J. Xin, "Advances and opportunities in passive wake-up radios with wireless energy harvesting for the Internet of Things applications," *Sensors*, vol. 19, no. 14, p. 3078, Jul. 2019.
- [9] U. Muncuk, K. Alemdar, J. D. Sarode, and K. R. Chowdhury, "Multiband ambient RF energy harvesting circuit design for enabling batteryless sensors and IoT," *IEEE Internet Things J.*, vol. 5, no. 4, pp. 2700–2714, Aug. 2018.
- [10] Z. Ye et al., "A breathable, reusable, and zero-power smart face mask for wireless cough and mask-wearing monitoring," *ACS Nano*, vol. 16, no. 4, pp. 5874–5884, Apr. 2022.
- [11] L. Zhu, T. D. Ha, Y.-H. Chen, H. Huang, and P.-Y. Chen, "A passive smart face mask for wireless cough monitoring: A harmonic detection scheme with clutter rejection," *IEEE Trans. Biomed. Circuits Syst.*, vol. 16, no. 1, pp. 129–137, Feb. 2022.
- [12] A. Dionisi, D. Marioli, E. Sardini, and M. Serpelloni, "Autonomous wearable system for vital signs measurement with energy-harvesting module," *IEEE Trans. Instrum. Meas.*, vol. 65, no. 6, pp. 1423–1434, Jun. 2016.
- [13] H. Ozkan, O. Ozhan, Y. Karadana, M. Gulcu, S. Macit and F. Husain, "A Portable Wearable Tele-ECG Monitoring System," in *IEEE Transactions on Instrumentation and Measurement*, vol. 69, no. 1, pp. 173–182, Jan. 2020.
- [14] S. Ladan, A. B. Guntupalli, and K. Wu, "A high-efficiency 24 GHz rectenna development towards millimeter-wave energy harvesting and wireless power transmission," *IEEE Trans. Circuits Syst.*, vol. 61, no. 12, pp. 3358–3366, 2014.
- [15] B. Strassner and K. Chang, "5.8-GHz circularly polarized rectifying antenna for wireless microwave power transmission," *IEEE Trans. Microw. Theory Techn.*, vol. 50, no. 8, pp. 1870–1876, Aug. 2002.
- [16] Y.-J. Ren and K. Chang, "5.8-GHz circularly polarized dual-diode rectenna and rectenna array for microwave power transmission," *IEEE Trans. Microw. Theory Techn.*, vol. 54, no. 4, pp. 1495–1502, 2006.
- [17] E. Kwiatkowski, J. A. Estrada, A. Lopez-Yela, and Z. Popovic, "Broadband RF energy-harvesting arrays," *Proc. IEEE*, vol. 110, no. 1, pp. 74–88, Jan. 2022.
- [18] M. Pinuela, P. D. Mitcheson, and S. Lucyszyn, "Ambient RF energy harvesting in urban and semiurban environments," *IEEE Trans. Microw. Theory Techn.*, vol. 61, no. 7, pp. 2715–2726, Jul. 2013.
- [19] C. Song et al., "A novel six-band dual CP rectenna using improved impedance matching technique for ambient RF energy harvesting," *IEEE Trans. Antennas Propag.*, vol. 64, no. 7, pp. 3160–3171, Jul. 2016.
- [20] Z. Popović, E. A. Falkenstein, D. Costinett, and R. Zane, "Low-power far-field wireless powering for wireless sensors," *Proc. IEEE*, vol. 101, no. 6, pp. 1397–1409, Jun. 2013.
- [21] A. Dolgov, R. Zane, and Z. Popovic, "Power management system for online low power RF energy harvesting optimization," *IEEE Trans. Circuits Syst. I, Reg. Papers*, vol. 57, no. 7, pp. 1802–1811, Jul. 2010.
- [22] S. Shen, Y. Zhang, C.-Y. Chiu, and R. Murch, "An ambient RF energy harvesting system where the number of antenna ports is dependent on frequency," *IEEE Trans. Microw. Theory Techn.*, vol. 67, no. 9, pp. 3821–3832, 2019.
- [23] T.D. Ha, X. C. Nie., M. Akinsolu, B. Liu, and P-Y. Chen, "An artificial intelligence-assisted optimization of imperceptible multi-mode rectenna," *IEEE Antennas Wireless Propag. Lett.*, 2024, submitted.
- [24] D. H. N. Bui, T. Vuong, J. Verdier, B. Allard, and P. Benech, "Design and measurement of 3D flexible antenna diversity for ambient RF energy scavenging in indoor scenarios," *IEEE Access*, vol. 7, pp. 17033–17044, 2019.
- [25] Y.-S. Chen and J.-W. You, "A scalable and multidirectional rectenna system for RF energy harvesting," *IEEE Trans. Compon., Packag., Manuf. Technol.*, vol. 8, no. 12, pp. 2060–2072, Dec. 2018.
- [26] M. Kumar, S. Kumar, and A. Sharma, "An Analytical Framework of Multisector Rectenna Array Design for Angular Misalignment Tolerant RF Power Transfer Systems," *IEEE Trans. Microw. Theory Techn.*, Early Access, pp.1-13, Dec. 2022.
- [27] H. Sun and W. Geyi, "A new rectenna using beamwidth-enhanced antenna array for RF power harvesting applications," *IEEE Antennas Wireless Propag. Lett.*, vol. 16, pp. 1451–1454, 2017.
- [28] M. Kumar, S. Kumar, and A. Sharma, "A Compact 3-D Multisector Orientation Insensitive Wireless Power Transfer System," *IEEE Antennas Wireless Propag. Lett.*, vol. 33, no.3, Mar. 2023.
- [29] J. Hagerty, F. Helmbrecht, W. McCalpin, R. Zane, and Z. Popovic, "Recycling ambient microwave energy with broad-band rectenna arrays," *IEEE Trans. Microw. Theory Techn.*, vol. 53, no. 3, pp. 1014–1024, Mar. 2004.
- [30] T.D. Ha, L. Zhu, N. AlSaab, P-Y. Chen, and J. L. Guo, "Optically transparent metasurface radome for RCS reduction and gain enhancement of multifunctional antennas," *IEEE Trans. Antennas Propag.*, vol. 71, no. 1, pp. 67-77, Jan. 2023.
- [31] T. S. Almoneef, F. Erkmen, M. A. Alotaibi, and O. M. Ramahi, "A new approach to micro-wave rectennas using tightly coupled antennas," *IEEE Trans. Antennas Propag.*, vol. 66, no. 4, pp. 1714–1724, 2018.
- [32] N. Shinohara and H. Matsumoto, "Experimental study of large rectenna array for microwave energy transmission," *IEEE Trans. Microw. Theory Techn.*, vol. 46, no. 3, pp. 261–268, 1998.
- [33] A. I. Sulyman et al., "Radio propagation path loss models for 5G cellular networks in the 28 GHz and 38 GHz millimeter-wave bands," *IEEE Commun. Mag.*, vol. 52, no. 9, pp. 78–86, Sep. 2014.
- [34] T. S. Rappaport, Y. Xing, G. R. MacCartney, A. F. Molisch, E. Mellios and J. Zhang, "Overview of Millimeter Wave Communications for Fifth-Generation (5G) Wireless Networks—With a Focus on Propagation Models," *IEEE Trans. Antennas Propag.*, vol. 65, no. 12, pp. 6213–6230, Dec. 2017.
- [35] Y. Hu, S. Sun, H. Xu, and H. Sun, "Grid-array rectenna with wide angle coverage for effectively harvesting RF energy of low power density," *IEEE Trans. Microw. Theory Techn.*, vol. 67, no. 1, pp. 402–413, Jan. 2019.
- [36] Y.-Y. Hu, S. Sun, H. Wu, S. Yang, and J. Hu, "Integrated coupler-antenna design for multibeam dual-polarized patch-array rectenna," *IEEE Trans. Antennas Propag.*, vol. 70, no. 3, pp. 1869–1883, Mar. 2022.
- [37] E. Vandelle, D. H. N. Bui, T.-P. Vuong, G. Ardila, K. Wu, and S. Hemour, "Harvesting ambient RF energy efficiently with optimal angular coverage," *IEEE Trans. Antennas Propag.*, vol. 67, no. 3, pp. 1862–1873, Mar. 2019.
- [38] A. Eid, J. G. D. Hester, and M. M. Tentzeris, "5G as a wireless power grid," *Sci. Rep.*, vol. 11, no. 1, p. 636, Dec. 2021.
- [39] T. H. Ha, L. Zhu, and P.-Y. Chen, "A low-cost wide-angle multi-beam coverage Bruce rectennas for energy harvesting applications," *Proc. IEEE Int. Symp. Antennas Propag. North Amer. Radio Sci. Meeting*, Jul. 2022, pp. 1–2.
- [40] Y.-J. Ren and K. Chang, "New 5.8 GHz circularly polarized retrodirective rectenna arrays for wireless power transmission," *IEEE Trans. Microw. Theory Techn.*, vol. 54, no. 7, pp. 2970–2976, Jul. 2006.
- [41] I. Afifi and A.-R. Sebak, "Wideband 4 × 4 Butler matrix in the printed ridge gap waveguide technology for millimeter wave applications," *IEEE Trans. Antennas Propag.*, vol. 68, no. 11, pp. 7670–7675, Nov. 2020.
- [42] C. Caloz and T. Itoh, *Electromagnetic Metamaterials: Transmission Line Theory and Microwave Applications*. Hoboken, NJ, USA: Wiley, 2005.
- [43] <https://www.skyworksinc.com/Products/Diodes/SMS7630-Series>
- [44] D. M. Pozar, *Microwave Engineering*, 4th ed. New York, NY, USA: Wiley, 2011, p. 101-102.
- [45] A. Balanis, *Antenna Theory: Analysis and Design* 4th ed. Hoboken, NJ, USA: Wiley, 2016, pp.88-90.